

KANAZAWA-16-12

LPT-Orsay-16-62

TUM-HEP-1070-16

Implications of Two-component Dark Matter Induced by Forbidden Channels and Thermal Freeze-out

Mayumi Aoki^{1*}, Takashi Toma^{2,3†}

¹*Institute for Theoretical Physics, Kanazawa University, Kanazawa 920-1192, Japan*

²*Laboratoire de Physique Théorique, CNRS,
Univ. Paris-Sud, Université Paris-Saclay, 91405 Orsay, France*

³*Physik-Department T30d, Technische Universität München,
James-Frank-Straße, D-85748 Garching, Germany*

Abstract

We consider a model of two-component dark matter based on a hidden $U(1)_D$ symmetry, in which relic densities of the dark matter are determined by forbidden channels and thermal freeze-out. The hidden $U(1)_D$ symmetry is spontaneously broken to a residual \mathbb{Z}_4 symmetry, and the lightest \mathbb{Z}_4 charged particle can be a dark matter candidate. Moreover, depending on the mass hierarchy in the dark sector, we have two-component dark matter. We show that the relic density of the lighter dark matter component can be determined by forbidden annihilation channels which require larger couplings compared to the normal freeze-out mechanism. As a result, a large self-interaction of the lighter dark matter component can be induced, which may solve small scale problems of Λ CDM model. On the other hand, the heavier dark matter component is produced by normal freeze-out mechanism. We find that interesting implications emerge between the two dark matter components in this framework. We explore detectabilities of these dark matter particles and show some parameter space can be tested by the SHiP experiment.

*mayumi@hep.s.kanazawa-u.ac.jp

†takashi.toma@tum.de

1 Introduction

There are some clear evidences for the existence of dark matter in the universe such as the rotation curves of spiral galaxies, the gravitational lensing effects, the cosmic microwave background (CMB) measurements, the large scale structure of the universe and the collision of the bullet clusters. From the view point of particle physics, the most well-known and promising dark matter candidate would be the Weakly Interacting Massive Particles (WIMPs) with the mass of electroweak to TeV scale. This kind of dark matter has been explored through direct, indirect and collider searches. However in spite of making a great effort to find WIMPs, any clear signal of WIMPs is not found yet.

Self-interactions of dark matter which are different from gravitational force may be a key to understand the nature of dark matter. Self-interactions may give a solution for the small scale problems of the standard cosmological model (the so-called Λ CDM model) such as the cusp-core, too-big-to-fail and missing satellites problems. The cusp-core problem is that the profile of dark matter inferred by N-body simulation with collisionless dark matter does not match with that estimated from the observation of the rotation curves of the spiral galaxies. The too-big-to-fail problem is that subhalos inferred by simulations with cold dark matter is too dense compared to the observations in the Milky Way. The missing satellites problem is that the predicted number of the subhalos in the local group is an order of magnitude more than the number of the observed satellites. The required magnitude of the self-interacting cross section in order to solve these problems is roughly given by $\sigma/m \sim 0.5 - 50 \text{ cm}^2/\text{g}$ where σ is the self-interacting cross section and m is the dark matter mass [1]. One should note that the collision of the bullet clusters gives an upper bound on the self-interacting cross section as $\sigma/m < 1.25 \text{ cm}^2/\text{g}$ [2]. Another implication of self-interacting dark matter is the recent observation of the cluster Abell 3827 at which it is measured an off-set of 1.62 kpc between the center of the dark matter sub-halo and the galaxy with 3.3σ confidence level [3]. This may be understood with a large self-interaction of dark matter, and the required magnitude of the self-interacting cross section is $\sigma/m \sim \mathcal{O}(1) \text{ cm}^2/\text{g}$ [3, 4].

Understanding such a large self-interaction of dark matter with typical WIMPs may be difficult since the ratio of cross section and dark matter mass σ/m is roughly scaled by $\sigma/m \propto m^{-3}$, thus the ratio σ/m sharply decreases with increasing dark matter mass. A Strongly Interacting Massive Particle (SIMP) is one of the good candidates which can have large self-interacting cross section [5–13].¹ In addition, the candidate which is a kind of WIMPless dark matter [14] produced by forbidden channels is another possibility to obtain a large self-interacting cross section [13, 15, 16].

On the other hand, although the dark matter existing in the universe is normally assumed to be occupied by one-component for simplicity, this assumption is not necessary

¹Introducing \mathbb{Z}_3 symmetry is the simplest extension of SIMP dark matter. Getting a large self-interacting cross section for the SIMP in a \mathbb{Z}_3 symmetric model, however, may not be easy consistently with perturbative couplings and potential stability [8].

and the dark matter can be composed of multi-particles in general. If multi-component dark matter is assumed, some interesting phenomenology is expected to occur. For example, if the second dark matter component is sub-dominant and has large self-interaction, this sub-dominant component may form a disk like the normal matter, which is discussed as Double Disk Dark Matter in Refs. [17, 18]. In this case, different properties for indirect and direct detection of dark matter would emerge. Other implications of multi-component dark matter also have been explored [19]. Some UV complete models with multi-component dark matter and its phenomenology have been explored based on the simplest \mathbb{Z}_4 symmetry [20], radiative neutrino masses [21–25], hidden gauge symmetries [26–28], $\mathbb{Z}_2 \times \mathbb{Z}_2$ symmetry [29], $\mathbb{Z}_2 \times U(1)_{PQ}$ symmetry [30], gauged $U(1)_{B-L}$ symmetry [31] and Kaluza-Klein theory [32].

In this paper, we consider a hidden $U(1)_D$ extension of the Standard Model (SM), which is spontaneously broken to the residual \mathbb{Z}_4 symmetry. Due to the remnant symmetry and an assumption of mass hierarchy, two particles in the dark sector can be stabilized. We discuss the two dark matter components in this model. The relic density of the lighter component can be determined by forbidden channels while that for the heavier component is fixed by thermal freeze-out. As a consequence, self-interacting cross section for the lighter dark matter can be large enough to solve the small scale problems. The two dark matter components are closely correlated with each other and those implications are also discussed.

This paper is organized as follows. In Section 2, details of the model are presented, and some basic constraints relevant to new particles are discussed. The relic density and self-interaction of two-component dark matter are discussed and numerically evaluated in Section 3. Section 4 is devoted to give detection properties of the two dark matter components. Summary and conclusions are given in Section 5.

2 The Model

We consider the model extended with the hidden $U(1)_D$ gauge symmetry. The new particle contents and the charge assignments of the $U(1)_D$ symmetry are shown in Tab. 1. The new complex scalar Σ which develops a vacuum expectation value (VEV), and two new inert complex scalars S and χ are introduced to the SM, where the $U(1)_D$ charge of Σ is normalized to 1. This normalization would be relevant to perturbativity of the $U(1)_D$ gauge coupling. Namely, the combination of the $U(1)_D$ charge and gauge coupling is bounded from above, and fixing the largest $U(1)_D$ charge in the hidden particles to be one would be reasonable to consider the perturbative gauge coupling. This model is automatically anomaly free since we add only new complex scalars. The kinetic terms of the new particles are given by

$$\mathcal{L} = |D_\mu \Sigma|^2 + |D_\mu S|^2 + |D_\mu \chi|^2 - \frac{\epsilon}{2} B_{\mu\nu} Z'^{\mu\nu}, \quad (1)$$

Table 1: New particle contents and $U(1)_D$ charges Q_D .

| | Σ | S | χ |
|------------------------|----------|------|--------|
| Q_D | 1 | -1/2 | 1/4 |
| Remnant \mathbb{Z}_4 | 0 | 2 | 1 |
| Spin | 0 | 0 | 0 |

where the covariant derivative is defined by $D_\mu \equiv \partial_\mu + iQ_D g_D Z'_\mu$ with the $U(1)_D$ charge Q_D given in Tab. 1 and the $U(1)_D$ gauge coupling constant g_D . The last term in Eq.(1) is the kinetic mixing between the $U(1)_Y$ and $U(1)_D$ gauge fields which gives the interaction between the SM and the hidden sector particles. In fact, non-zero kinetic mixing is required to ensure that the SM and the dark sector particles are in thermal (kinetic) equilibrium at the early universe.² The off-diagonal kinetic term given by the kinetic mixing ϵ can be diagonalized to obtain the physical mass eigenstates of the gauge bosons. The detailed discussion of the diagonalization has been given in Refs. [8, 11] for example. In particular, when a light Z' gauge boson ($m_{Z'} \ll m_Z$) is considered as we will see below, the matrix of the kinetic terms is diagonalized within good approximation with the following replacement

$$Z_\mu \rightarrow Z_\mu, \quad (2)$$

$$A_\mu \rightarrow A_\mu - \epsilon_\gamma Z'_\mu, \quad (3)$$

$$Z'_\mu \rightarrow Z'_\mu - \epsilon_\gamma \tan \theta_W Z_\mu, \quad (4)$$

where $\epsilon_\gamma \equiv \epsilon \cos \theta_W$ and θ_W is the Weinberg angle. The kinetic mixing ϵ_γ is experimentally constrained as $\epsilon_\gamma \lesssim 10^{-3}$ for $m_{Z'} \sim \text{MeV-GeV}$ as we will see later.

The full renormalizable scalar potential is written down as

$$\begin{aligned} \mathcal{V} = & \mu_\Phi^2 |\Phi|^2 + \mu_\Sigma^2 |\Sigma|^2 + \mu_S^2 |S|^2 + \mu_\chi^2 |\chi|^2 + \frac{\lambda_\Phi}{4} |\Phi|^4 + \frac{\lambda_\Sigma}{4} |\Sigma|^4 + \frac{\lambda_S}{4} |S|^4 + \frac{\lambda_\chi}{4} |\chi|^4 \\ & + \lambda_{\Phi\Sigma} |\Phi|^2 |\Sigma|^2 + \lambda_{\Phi S} |\Phi|^2 |S|^2 + \lambda_{\Phi\chi} |\Phi|^2 |\chi|^2 + \lambda_{\Sigma S} |\Sigma|^2 |S|^2 + \lambda_{\Sigma\chi} |\Sigma|^2 |\chi|^2 + \lambda_{S\chi} |S|^2 |\chi|^2 \\ & + \left(\frac{\kappa}{2} \Sigma S^2 + \frac{\mu}{2} S \chi^2 + \frac{\lambda}{2} \Sigma S \chi^{\dagger 2} + \text{H.c.} \right). \end{aligned} \quad (5)$$

We assume that only the SM Higgs doublet Φ and the new complex scalar Σ have VEVs ($\langle \Sigma \rangle \ll \langle \Phi \rangle$) as denoted by

$$\Phi = \begin{pmatrix} 0 \\ \langle \Phi \rangle + \phi^0 / \sqrt{2} \end{pmatrix}, \quad \Sigma = \langle \Sigma \rangle + \frac{\sigma}{\sqrt{2}}. \quad (6)$$

The $U(1)_D$ symmetry is spontaneously broken by the VEV of Σ , and the mass of Z' gauge boson is generated due to the symmetry breaking as

$$m_{Z'}^2 = g_D^2 \langle \Sigma \rangle^2. \quad (7)$$

²Thermal equilibrium between the SM and dark sectors may also be achieved with the couplings in the scalar potential. In this case, the extra Higgs boson denoted by H should be light enough in order to induce a sufficient reaction rate between the SM and dark sectors.

For hierarchical VEVs $\langle \Sigma \rangle \ll \langle \Phi \rangle$, a light Z' boson ($m_{Z'} \ll m_Z$) is obtained. In the scalar potential, the cubic term $(\kappa/2)\Sigma S^2$ induces a mass splitting between the CP-even and odd states of S after the $U(1)_D$ symmetry breaking. Their masses are given by

$$m_{s_R}^2 = \mu_S^2 + \lambda_{\Phi S} \langle \Phi \rangle^2 + \lambda_{\Sigma S} \langle \Sigma \rangle^2 + \kappa \langle \Sigma \rangle, \quad (8)$$

$$m_{s_I}^2 = \mu_S^2 + \lambda_{\Phi S} \langle \Phi \rangle^2 + \lambda_{\Sigma S} \langle \Sigma \rangle^2 - \kappa \langle \Sigma \rangle, \quad (9)$$

where S is decomposed as $S = (s_R + i s_I)/\sqrt{2}$. Hereafter we assume that the parameter κ is small, namely the mass splitting between s_R and s_I is small enough. However one should note that the parameter κ is bounded from below. It is relevant to the inelastic scattering for direct detection of dark matter s_I .³ If κ is small enough, the inelastic scattering with electron via the Z' gauge boson exchange $s_I e^- \rightarrow s_R e^-$ may give a constraint on this model. In order to evade this inelastic scattering, the parameter κ is constrained as $\kappa \gtrsim m_{s_I} v^2/2$ where $m_{s_I} \approx \langle \Sigma \rangle \gg m_{s_R} - m_{s_I}$ is assumed. Here $v \sim 10^{-3}$ is the dark matter velocity in the present universe. Thus for example, if $m_{s_I} \sim 200$ MeV, the lower bound for κ is given by $\kappa \gtrsim 100$ eV. Another lower bound of the parameter κ is induced from Big Bang Nucleosynthesis (BBN). This is because the successful BBN is spoiled if the CP-even state s_R has a too long lifetime ($\tau_{s_R} \gtrsim 0.1$ s) [33, 34]. Assuming $m_{s_R} - m_{s_I} \gg m_e$, the decay width of s_R can roughly be computed as

$$\Gamma_{s_R \rightarrow s_I e^+ e^-} \approx \frac{\epsilon_\gamma^2 \alpha_{\text{em}}}{192 \pi^2 g_D} \frac{\kappa^3}{m_{s_I} m_{Z'}}. \quad (10)$$

From this formula, fixing $m_{s_I} \approx m_{Z'}/2$, $g_D = 1$, $\epsilon_\gamma = 10^{-7}$ for example, the lower bound of κ is derived as

$$\kappa \gtrsim 10 \text{ MeV} \times \left(\frac{m_{Z'}}{100 \text{ MeV}} \right)^{2/3}. \quad (11)$$

Therefore one can see that the BBN constraint is stronger and we take the parameter κ satisfying the BBN constraint in the following discussion. When the relic density of the dark matter is computed, we can neglect the mass difference between s_R and s_I , and thus S is regarded as a complex scalar particle because s_R and s_I are thermalized in the early universe. On the other hand, the mass difference cannot be neglected when detection properties such as direct and indirect detection rates are computed in the current universe.

The mass of χ is given by

$$m_\chi^2 = \mu_\chi^2 + \lambda_{\Phi\chi} \langle \Phi \rangle^2 + \lambda_{\Sigma\chi} \langle \Sigma \rangle^2. \quad (12)$$

The neutral component of the SM Higgs doublet ϕ^0 and the scalar σ in the dark sector mix with each other, and the mass matrix can be diagonalized as

$$\begin{aligned} \mathcal{V} &\supset \frac{1}{2} \begin{pmatrix} \phi^0 & \sigma \end{pmatrix} \begin{pmatrix} \lambda_\Phi \langle \Phi \rangle^2 & 2\lambda_{\Phi\Sigma} \langle \Phi \rangle \langle \Sigma \rangle \\ 2\lambda_{\Phi\Sigma} \langle \Phi \rangle \langle \Sigma \rangle & \lambda_\Sigma \langle \Sigma \rangle^2 \end{pmatrix} \begin{pmatrix} \phi^0 \\ \sigma \end{pmatrix} \\ &= \frac{1}{2} \begin{pmatrix} h & H \end{pmatrix} \begin{pmatrix} m_h^2 & 0 \\ 0 & m_H^2 \end{pmatrix} \begin{pmatrix} h \\ H \end{pmatrix}, \end{aligned} \quad (13)$$

³The CP-odd scalar s_I is identified as one of the two dark matter components with the mass below GeV scale.

where the minimum conditions of the scalar potential are imposed. The mass eigenstates h and H are understood as the SM-like Higgs boson with $m_h = 125$ GeV and an extra (dark) Higgs boson, respectively. The gauge eigenstates ϕ^0 and σ can be rewritten by the mass eigenstates as

$$\begin{pmatrix} \phi^0 \\ \sigma \end{pmatrix} = \begin{pmatrix} \cos \alpha & -\sin \alpha \\ \sin \alpha & \cos \alpha \end{pmatrix} \begin{pmatrix} h \\ H \end{pmatrix} \quad \text{with} \quad \sin 2\alpha = \frac{4\lambda_{\Phi\Sigma}\langle\Phi\rangle\langle\Sigma\rangle}{m_h^2 - m_H^2}. \quad (14)$$

The mixing angle $\sin \alpha$ is constrained by the electroweak precision data, Higgs coupling measurements and direct search for a new scalar, and the current bound is given by $\sin \alpha \lesssim 0.01$ for $m_H \lesssim 5$ GeV [35, 36]. In this mass region, the strongest bound is given by the decay mode $B \rightarrow K\ell\ell$ [37–40]. Since the mass of the extra Higgs boson H is basically given by $m_H^2 \sim 4\lambda_{\Phi\Sigma}^2\langle\Sigma\rangle^2/\lambda_\Phi$ where $\lambda_\Sigma\langle\Sigma\rangle \ll \lambda_{\Phi\Sigma}\langle\Phi\rangle$ is assumed, the scale of m_H is correlated with $m_{Z'}$ like $m_H^2/m_{Z'}^2 \sim 4\lambda_{\Phi\Sigma}^2/(\lambda_\Phi g_D^2)$. Therefore, if the gauge coupling is taken as $g_D \sim 1$, the mass m_H cannot be much larger than $m_{Z'}$ due to the perturbativity of the couplings.

The invisible decay of the SM-like Higgs boson h also gives a constraint on the quartic couplings in the scalar potential. The current upper bound of the branching fraction into the invisible decay mode is given as $\text{Br}(h \rightarrow \text{inv}) \leq 0.28$ [41] by the ATLAS Collaboration and $\text{Br}(h \rightarrow \text{inv}) \leq 0.24$ [42] by the CMS Collaboration at 95% confidence level. If the value of the ATLAS Collaboration is taken as a conservative limit, this upper bound can be translated into the upper bound of the invisible decay width as $\Gamma_{\text{inv}} \leq 1.6$ MeV where $\Gamma_h^{\text{SM}} = 4.1$ MeV is used [43]. In this model, the possible invisible decay channels are given by $h \rightarrow HH, s_R s_R, s_I s_I, (\chi\chi^\dagger)$ and each decay width is computed as

$$\Gamma_{HH} = \frac{\mu_{hHH}^2}{32\pi m_h} \sqrt{1 - \frac{4m_H^2}{m_h^2}}, \quad (15)$$

$$\Gamma_{SS^\dagger} = \frac{\mu_{hSS^\dagger}^2}{16\pi m_h} \sqrt{1 - \frac{4m_S^2}{m_h^2}}, \quad (16)$$

$$\Gamma_{\chi\chi^\dagger} = \frac{\mu_{h\chi\chi^\dagger}^2}{16\pi m_h} \sqrt{1 - \frac{4m_\chi^2}{m_h^2}}, \quad (17)$$

with

$$\begin{aligned} \mu_{hHH} &\equiv \frac{\sin \alpha \cos \alpha}{\sqrt{2}} \left(\lambda_\Phi \langle\Phi\rangle \sin \alpha + \lambda_\Sigma \langle\Sigma\rangle \cos \alpha \right) \\ &\quad + \sqrt{2} \lambda_{\Phi\Sigma} \left(\langle\Phi\rangle \cos \alpha (1 - 3 \sin^2 \alpha) + \langle\Sigma\rangle \sin \alpha (1 - 3 \cos^2 \alpha) \right), \end{aligned} \quad (18)$$

$$\mu_{hSS^\dagger} \equiv \sqrt{2} \left(\lambda_{\Phi S} \langle\Phi\rangle \cos \alpha + \lambda_{\Sigma S} \langle\Sigma\rangle \sin \alpha \right), \quad (19)$$

$$\mu_{h\chi\chi^\dagger} \equiv \sqrt{2} \left(\lambda_{\Phi\chi} \langle\Phi\rangle \cos \alpha + \lambda_{\Sigma\chi} \langle\Sigma\rangle \sin \alpha \right), \quad (20)$$

where since the CP-even and odd states s_R and s_I are nearly degenerate, these contributions are approximated by Γ_{SS^\dagger} . Thus if all the hidden particles are much lighter than

the SM-like Higgs boson, the couplings are constrained as

$$\mu_{hHH}^2 + 2\mu_{hSS^\dagger}^2 + 2\mu_{h\chi\chi^\dagger}^2 \lesssim 4.5 \text{ GeV}. \quad (21)$$

In the following analysis, we discuss parameter regions in which the above constraints are satisfied.

In this model, a remnant \mathbb{Z}_4 symmetry remains after the $U(1)_D$ symmetry breaking as one can see from Tab. 1. Due to this \mathbb{Z}_4 symmetry, the decay of χ is forbidden and thus χ can be a dark matter candidate. Moreover, depending on the mass hierarchy, we may have a second dark matter component s_I because the decay of s_I is forbidden if $m_{s_I} \leq 2m_\chi$ is satisfied. In the following, we consider two-component dark matter composed of s_I and χ with the mass hierarchy $m_{s_I} (\approx m_{s_R}) \lesssim m_{Z'}, m_H < m_\chi$. In particular, we are interested in the mass region of $m_{s_I} \lesssim \mathcal{O}(100)$ MeV and $m_\chi \gtrsim 1$ GeV for large self-interaction induced by the lighter component s_I . There are two kinds of interactions between dark matter and the SM particles which are the gauge coupling g_D and the Higgs couplings in the scalar potential. Both interactions would play an important role for dark matter phenomenology. Note that a certain degree of parameter tuning is needed to achieve the hierarchical masses between the two dark matter components in this model.⁴ The magnitude of the tuning would be the same order as that in the SM in which one needs a tuning in order to obtain the hierarchical fermion masses.

3 Dark Matter

3.1 Relic Density

In general, the coupled Boltzmann equations for two-component dark matter S and χ should be solved in order to compute the relic densities since in addition to the standard annihilation processes, various processes such as co-annihilations, semi-annihilations and conversion processes between two dark matter components should be taken into account.⁵ For example, the semi-annihilation processes $\chi\chi \rightarrow SH, Sh$ occur if the quartic coupling λ is large enough, however these processes and the other semi-annihilation processes can be neglected by assuming small couplings κ, μ and λ . Since we focus on a large mass hierarchy between two dark matter species ($m_S \ll m_\chi$), the equations are almost decoupled and given by

$$\frac{dn_S}{dt} + 3Hn_S = -\frac{1}{2}\langle\sigma_S v\rangle \left[n_S^2 - n_S^{\text{eq}2}\right], \quad (22)$$

$$\frac{dn_\chi}{dt} + 3Hn_\chi = -\frac{1}{2}\langle\sigma_\chi v\rangle \left[n_\chi^2 - n_\chi^{\text{eq}2}\right]. \quad (23)$$

⁴Although it is difficult to derive theoretically such a large mass hierarchy within this model, it may be achieved in different frameworks such as global $U(1)$ models in which the pseudo-Goldstone boson can be identified as a lighter dark matter candidate corresponding to s_I .

⁵As mentioned above, the complex scalar S can be effectively regarded as a dark matter particle in the early universe since the mass splitting between s_R and s_I is very small.

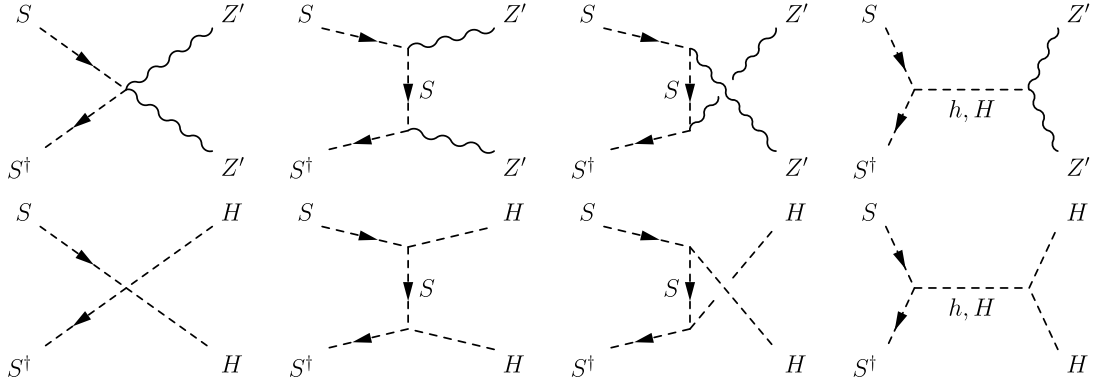


Figure 1: Diagrams for the s_R, s_I forbidden channels ($m_{s_R}, m_{s_I} < m_{Z'}, m_H$).

Thus one can independently solve the Boltzmann equations for each dark matter particle. The heavier state χ would firstly decouple from the thermal bath before the decoupling of the lighter state S . This is naively expected since the mass hierarchy among the two dark matter particles are sufficiently large. The number densities n_S and n_χ are defined by the total number densities of (S, S^\dagger) and (χ, χ^\dagger) , respectively. Because of this, the factor $1/2$ in front of the cross sections appears in Eq. (22) and (23). The thermally averaged cross sections $\langle \sigma_{Sv} \rangle$ and $\langle \sigma_\chi v \rangle$ should include all the possible annihilation channels. The two dark matter components should have comparable relic density, otherwise this model can be effectively regarded as one-component dark matter model. The criterion for the range of the dark matter fraction is controversial. In this paper, we consider the fraction of each dark matter component should be larger than 10%.

3.1.1 Relic Density of S

The possible annihilation channel for the lighter dark matter state S is $SS^\dagger \rightarrow f\bar{f}$ where f is a SM fermion. However this process is suppressed by the small kinetic mixing $\epsilon_\gamma \lesssim 10^{-3}$ or the Higgs mixing $\sin \alpha$, thus cannot reproduce the observed relic density. In addition, since we consider the case of $m_S < m_{Z'}, m_H$, one may think the annihilation processes $SS^\dagger \rightarrow Z'Z', HH$ are kinematically forbidden. However the thermally averaged annihilation cross sections for these processes are not exactly zero because particles in the early universe have an energy distribution like the Maxwell-Boltzmann distribution. Thus it is possible to reproduce the correct relic density by the forbidden channels [13, 15, 16, 44]. The thermally averaged annihilation cross sections for the forbidden channels are suppressed by the Boltzmann factor, thus the order of the magnitude of the couplings required to reproduce the correct relic density would be larger than the case of normal WIMPs.

In this model, the relevant diagrams for the forbidden channels $SS^\dagger \rightarrow Z'Z', HH$ are shown in Fig. 1. Assuming CP invariance, the thermally averaged annihilation cross

section for the process $SS^\dagger \rightarrow XX$ can be written with the opposite process as [15]

$$\langle \sigma v \rangle_{SS^\dagger \rightarrow XX} = \langle \sigma v \rangle_{XX \rightarrow SS^\dagger} \left(\frac{2n_X^{\text{eq}}}{n_S^{\text{eq}}} \right)^2 = \langle \sigma v \rangle_{XX \rightarrow SS^\dagger} \frac{g_X^2 m_X^3}{m_S^3} e^{-2\Delta_X z_S}, \quad (24)$$

where $X = Z'$ or H , g_X is the degrees of freedom for X ($g_{Z'} = 3$ and $g_H = 1$), $\Delta_X = (m_X - m_S)/m_S$ and $z_S = m_S/T$. The factor 2 in the middle of Eq. (24) appears because we defined n_S as the total number density of S and S^\dagger . Each cross section $\langle \sigma v \rangle_{XX \rightarrow SS^\dagger}$ for $X = Z'$ and H is given by

$$\langle \sigma v \rangle_{Z'Z' \rightarrow SS^\dagger} \approx \frac{1}{72\pi m_{Z'}^2} \left(\frac{g_D}{2} \right)^4 \left[11 - 24 \frac{m_S^2}{m_{Z'}^2} + 16 \frac{m_S^4}{m_{Z'}^4} + 3(C_R^2 + C_I^2) - 2C_R \left(1 - 4 \frac{m_S^2}{m_{Z'}^2} \right) \right] \sqrt{1 - \frac{m_S^2}{m_{Z'}^2}}, \quad (25)$$

$$\langle \sigma v \rangle_{HH \rightarrow SS^\dagger} \approx \frac{1}{32\pi m_H^2} \left| \lambda_{HSS^\dagger} - \frac{2\mu_{HSS^\dagger}^2}{m_H^2} + \frac{\mu_{HHH} \mu_{HSS^\dagger}}{3m_H^2 + im_H \Gamma_H} \right|^2 \sqrt{1 - \frac{m_S^2}{m_H^2}}, \quad (26)$$

in the non-relativistic limit ($v \rightarrow 0$). The new parameters in Eq. (25) and (26) are defined by

$$C_R \equiv \frac{4\sqrt{2} \cos \alpha}{g_D} \frac{\mu_{HSS^\dagger} m_{Z'} (4m_{Z'}^2 - m_H^2)}{(4m_{Z'}^2 - m_H^2)^2 + m_H^2 \Gamma_H^2}, \quad (27)$$

$$C_I \equiv -\frac{4\sqrt{2} \cos \alpha}{g_D} \frac{\mu_{HSS^\dagger} m_{Z'} m_H \Gamma_H}{(4m_{Z'}^2 - m_H^2)^2 + m_H^2 \Gamma_H^2}, \quad (28)$$

$$\lambda_{HSS^\dagger} \equiv \lambda_{\Phi S} \sin^2 \alpha + \lambda_{\Sigma S} \cos^2 \alpha, \quad (29)$$

$$\mu_{HSS^\dagger} \equiv \sqrt{2} \left(-\lambda_{\Phi S} \langle \Phi \rangle \sin \alpha + \lambda_{\Sigma S} \langle \Sigma \rangle \cos \alpha \right), \quad (30)$$

$$\begin{aligned} \mu_{HHH} \equiv & -\frac{3}{\sqrt{2}} \left(-\lambda_{\Phi} \langle \Phi \rangle \sin^3 \alpha + \lambda_{\Sigma} \langle \Sigma \rangle \cos^3 \alpha \right) \\ & + \frac{6}{\sqrt{2}} \lambda_{\Phi \Sigma} \sin \alpha \cos \alpha \left(-\langle \Phi \rangle \cos \alpha + \langle \Sigma \rangle \sin \alpha \right). \end{aligned} \quad (31)$$

The decay width for the extra Higgs boson H is given by $\Gamma_H = \Gamma_{Z'Z'} + \Gamma_{SS^\dagger} + \Gamma_{e\bar{e}} (+\Gamma_{\mu\bar{\mu}})$. Each decay width is computed as

$$\Gamma_{f\bar{f}} = \frac{y_f^2 \sin^2 \alpha m_H}{16\pi} \left(1 - 4 \frac{m_f^2}{m_H^2} \right)^{3/2}, \quad (32)$$

$$\Gamma_{Z'Z'} = \frac{g_D^2 \cos^2 \alpha m_{Z'}^2}{4\pi m_H} \left(3 - \frac{m_H^2}{m_{Z'}^2} + \frac{1}{4} \frac{m_H^4}{m_{Z'}^4} \right) \sqrt{1 - 4 \frac{m_{Z'}^2}{m_H^2}}, \quad (33)$$

$$\Gamma_{SS^\dagger} \approx \frac{\mu_{HSS^\dagger}^2}{16\pi m_H} \sqrt{1 - 4 \frac{m_S^2}{m_H^2}}, \quad (34)$$

where y_f is the SM Yukawa coupling for the fermion f . The relic density of the lighter dark matter particle S can be determined by solving the Boltzmann equation in Eq. (22) with sum of these cross sections for the forbidden channels.

In the above computation of the relic density, the thermal equilibrium between the dark sector and the SM sector is implicitly assumed. The condition for (kinetic) thermal equilibrium is given by $\Gamma_{\text{kin}} > H$ at the freeze-out temperature of dark matter s_I where H is the Hubble parameter and Γ_{kin} is defined by $\Gamma_{\text{kin}} \equiv \langle \sigma_{\text{el}} v \rangle n_{\text{SM}}$ with the elastic scattering cross section $\sigma_{\text{el}} v$ and the number density of the SM particles n_{SM} . The most relevant scattering process would be $s_I e^\pm \rightarrow s_I e^\pm$ or $s_I \mu^\pm \rightarrow s_I \mu^\pm$ through the t -channel diagram mediated by the extra Higgs boson H depending on the dark matter mass m_{s_I} . Since the cross section is suppressed by the small mixing angle $\sin \alpha$ and the electron Yukawa coupling for the case of scattering with e^\pm , the scattering cross section $\sigma_{\text{el}} v$ could be too small to keep the thermal equilibrium. If the condition for thermal equilibrium is not satisfied, the temperature of the dark sector would differentiate from that of the SM sector, and it could make the above computation change if the difference of the temperature is large enough.

In some parameter space, the 3-to-2 annihilation processes like $SSS^\dagger \rightarrow SZ'$ may be relevant in the mass range we focus on. Such a process may compete with the forbidden channels discussed above. If the 3-to-2 annihilation processes are dominant and the relic density is determined by these processes, the dark matter particle S would be identified as a so-called SIMP candidate [5–8, 10, 12]. Since considering a SIMP dark matter candidate in this model requires a certain degree of parameter tuning so that the 3-to-2 processes become dominant, we do not consider this possibility.

3.1.2 Relic Density of χ

For the heavier dark matter particle χ , three annihilation channels into the particles in the dark sector $\chi\chi^\dagger \rightarrow Z'Z', SS^\dagger, HH$ exist. The relevant diagrams for the annihilation channel $\chi\chi^\dagger \rightarrow Z'Z'$ are shown in the top of Fig. 2. The annihilation cross section is given by

$$\sigma v_{\chi\chi^\dagger \rightarrow Z'Z'} \approx \frac{1}{16\pi m_\chi^2} \left(\frac{g_D}{4} \right)^4 \frac{8m_\chi^4 - 8m_\chi^2 m_{Z'}^2 + 3m_{Z'}^4}{(m_{Z'}^2 - 2m_\chi^2)^2} \sqrt{1 - \frac{m_{Z'}^2}{m_\chi^2}}, \quad (35)$$

in the non-relativistic limit ($v \rightarrow 0$) where the contribution of the s -channel diagrams mediated by the Higgs bosons h, H can be neglected with small couplings $\lambda_{\Phi\chi}, \lambda_{\Sigma\chi} \ll 1$. In fact, such small couplings are required to evade the strong constraint of the dark matter direct detection experiments. The annihilation channel $\chi\chi^\dagger \rightarrow HH$ in the second line of Fig. 2 and the channels into the SM particles also exist. These may affect to the computation of the relic density of χ , however these channels can be regarded as subdominant compared to the channel $\chi\chi^\dagger \rightarrow Z'Z'$ due to $\lambda_{\Phi\chi}, \lambda_{\Sigma\chi} \ll 1$. The additional annihilation process $\chi\chi^\dagger \rightarrow SS^\dagger$ shown in the bottom of Fig. 2 may also be relevant, and

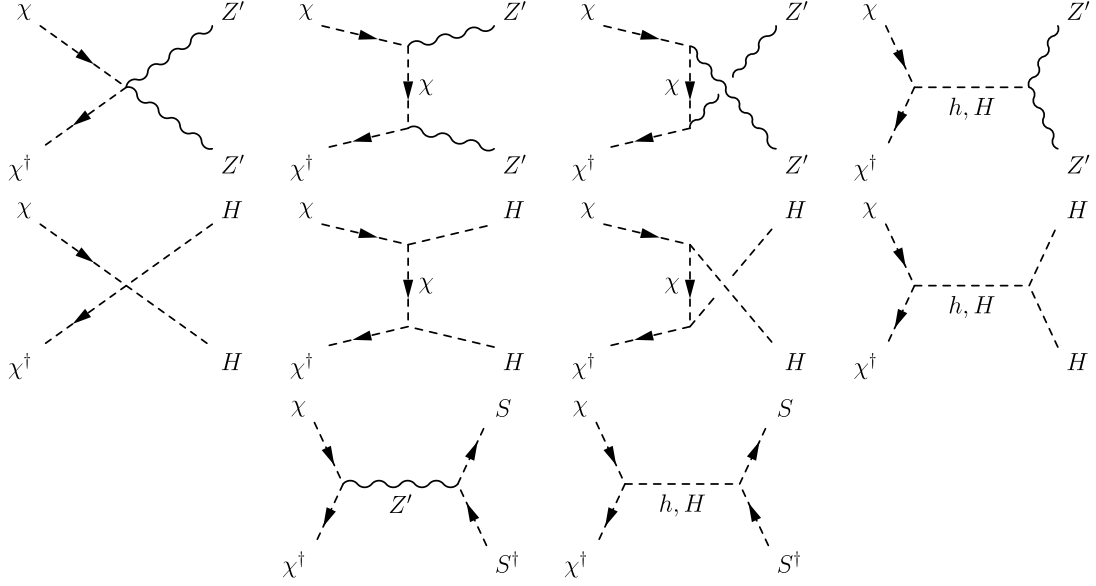


Figure 2: Diagrams for the χ annihilation.

the annihilation cross section for this process can be computed as

$$\sigma v_{\chi\chi^\dagger \rightarrow SS^\dagger} \approx \frac{1}{6\pi m_\chi^2} \left(\frac{g_D}{4}\right)^4 \left(1 - \frac{m_S^2}{m_\chi^2}\right)^{3/2} \frac{m_\chi^4 v^2}{(4m_\chi^2 - m_{Z'}^2)^2 + m_{Z'}^2 \Gamma_{Z'}^2}. \quad (36)$$

However as one can see from the formula, the annihilation cross section is suppressed by the dark matter relative velocity v , thus this contribution to the total annihilation cross section would be sub-dominant.

For the heavier dark matter χ , one should take into account the non-perturbative effect which is so-called Sommerfeld effect if the Z' gauge boson is much lighter than the dark matter particle χ as in our case. In this case, the wave function of the two dark matter particles in the initial state is distorted by long-range force, and the annihilation cross section would be enhanced [45–49]. The Sommerfeld enhancement factor can be obtained by solving the Schrödinger equation for the two body dark matter state $\psi(r)$ which is given by

$$-\frac{1}{m_\chi} \frac{d^2\psi}{dr^2} + V\psi = \frac{m_\chi v^2}{4}\psi, \quad \text{where} \quad V = -\frac{\alpha_{Z'}}{16r} e^{-m_{Z'}r}, \quad (37)$$

with $\alpha_{Z'} = g_D^2/(4\pi)$. Here r is the distance between the two dark matter particles. This Schrödinger equation is solved under the boundary condition $d\psi/dr(\infty) = 0$ and $\psi(0) = 1$, and then the Sommerfeld factor is given by $S_F \equiv |\psi(\infty)|^2$. An approximate analytic solution for the Schrödinger equation is given by [50]

$$S_F = \frac{\pi}{16\xi_v} \frac{\sinh\left(\frac{2\pi\xi_v}{\pi^2\xi_{Z'}/6}\right)}{\cosh\left(\frac{2\pi\xi_v}{\pi^2\xi_{Z'}/6}\right) - \cos\left(2\pi\sqrt{\frac{1}{16\pi^2\xi_{Z'}/6} - \frac{\xi_v^2}{(\pi^2\xi_{Z'}/6)^2}}\right)}, \quad (38)$$

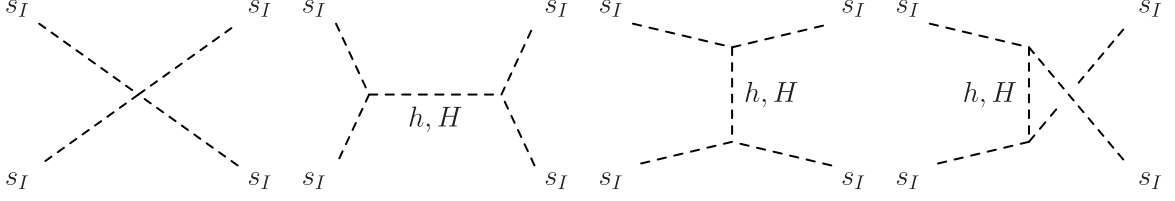


Figure 3: Diagrams for the self-interaction process $s_I s_I \rightarrow s_I s_I$.

where $\xi_v = v/(2\alpha_{Z'})$ and $\xi_{Z'} = m_{Z'}/(\alpha_{Z'} m_\chi)$. We use this formula in numerical calculations below. Thus the thermally average annihilation cross section for the channel $\chi\chi^\dagger \rightarrow Z'Z'$ with the Sommerfeld effect is given by

$$\langle\sigma v\rangle_{\chi\chi^\dagger\rightarrow Z'Z'} = \frac{z_\chi^{3/2}}{2\sqrt{\pi}} \int_0^\infty (\sigma v_{\chi\chi^\dagger\rightarrow Z'Z'}) S_F v^2 e^{-\frac{z_\chi v^2}{4}} dv, \quad (39)$$

where $z_\chi = m_\chi/T$. One can see that when $S_F = 1$ in Eq. (39), the formula without the Sommerfeld effect is recovered [44].

3.2 Self-interacting Cross Section

Strong self-interaction of dark matter is required in order to solve the small scale problems: cusp-core, too-big-to-tail and missing satellites problems. The required magnitude of the self-interacting cross section is quite large as $\sigma/m \sim 0.5 - 50 \text{ cm}^2/\text{g}$ [1]. Reproducing such a large self-interacting cross section may be difficult for the dark matter with above electroweak scale mass. However it is possible to achieve it if the mass of dark matter is below GeV scale, and we have such a candidate s_I in this model.

The self-interacting cross section for s_I is given by the process $s_I s_I \rightarrow s_I s_I$ whose complete diagrams are shown in Fig. 3, and is computed as

$$\sigma_{s_I s_I \rightarrow s_I s_I} \approx \frac{1}{128\pi m_{s_I}^2} \left| \frac{3}{2} \lambda_S - \frac{2\mu_{H s_I s_I}^2}{m_H^2} + \frac{\mu_{H s_I s_I}^2}{4m_{s_I}^2 - m_H^2 + im_H \Gamma_H} \right|^2, \quad (40)$$

where $\mu_{H s_I s_I}$ is given by $\mu_{H S S^\dagger}$ in Eq. (30) for $\kappa \approx 0$, and the contribution of the SM-like Higgs boson is neglected. Note that only the Higgs couplings contribute to the self-interacting cross section at the tree level. The gauge coupling does not give a contribution because it gives only an inelastic scattering cross section $s_I s_I \rightarrow s_R s_R$.

Since two dark matter components exist in this model, the required value of the self-interacting cross section for solving the small scale problems is scaled by the fraction of the s_I component in the total dark matter relic density. Thus it would be convenient to define the effective self-interacting cross section with

$$\sigma_{\text{self}}^{\text{eff}} = \left(\frac{\Omega_{s_I}}{\Omega_{\text{exp}}} \right)^2 \sigma_{s_I s_I \rightarrow s_I s_I}, \quad (41)$$

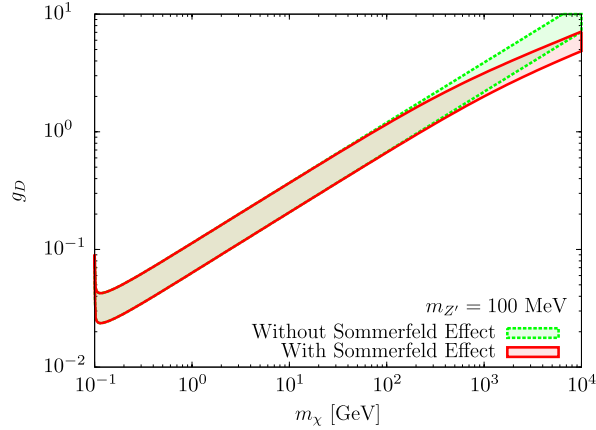


Figure 4: Parameter space reproducing the relic density of χ within $0.1 < f_\chi < 0.9$ in the plane (m_χ, g_D) where $m_{Z'}$ is fixed to be $m_{Z'} = 100$ MeV as an example.

where the parameters Ω_{s_I} and $\Omega_{\text{exp}} \approx 0.12/h^2$ (h is the dimensionless Hubble constant at the current time) are the relic density of s_I and the experimentally observed total dark matter relic density, respectively.

The self-interacting cross section for the heavier dark matter state χ can also be computed in the same way as the dark matter s_I . Since the cross section decreases as the dark matter mass increases, the cross section for the heavier state χ is expected to be small. Even if the mass of χ is larger than the electroweak scale, the self-interacting cross section may be enhanced by the Sommerfeld effect [51, 52]. However since the effect is not so important for the parameter space we are interested in, we neglect it.

3.3 Numerical Computations

The relic density and self-interacting cross section can numerically be computed. Fig. 4 shows the parameter space where the fraction $f_\chi \equiv \Omega_\chi/\Omega_{\text{exp}}$ gives $0.1 < f_\chi < 0.9$ in the plane of (m_χ, g_D) for $m_{Z'} = 100$ MeV. The red and the green regions respectively give the results with and without the Sommerfeld effect. One can see that the Sommerfeld effect becomes effective when $m_\chi \gtrsim 100$ GeV, which makes the required value of g_D smaller.⁶

In the left plots in Fig. 5, the contours generating the centre value of the observed relic density $\Omega_{s_I}h^2 + \Omega_\chi h^2 = 0.12$ are shown in the plane of $(m_{s_I}, \Delta_{Z'})$ where the dark matter mass m_χ is fixed to be $m_\chi = 5$ GeV in the upper panel and $m_\chi = 400$ GeV in the lower panel. The other relevant parameters are fixed to be $\lambda_S = \lambda_{\Sigma S} = 2$ and $\Delta_H = 1.1$. The quartic couplings $\lambda_{\Phi\Sigma}$ and $\lambda_{\Phi S}$ should be small enough to evade the constraint of the Higgs invisible decay, and λ_Σ should be taken such that $\lambda_\Sigma \langle \Sigma \rangle \ll \lambda_{\Phi\Sigma} \langle \Phi \rangle$ for the reasonable mass matrix in the upper line of Eq. (13). Each line of red, green and blue corresponds to $f_\chi = 0.1, 0.5$ and 0.9 , respectively. When the Z' gauge boson mass is light

⁶Implications of such a Sommerfeld effect on BBN and CMB have been discussed in [53–56].

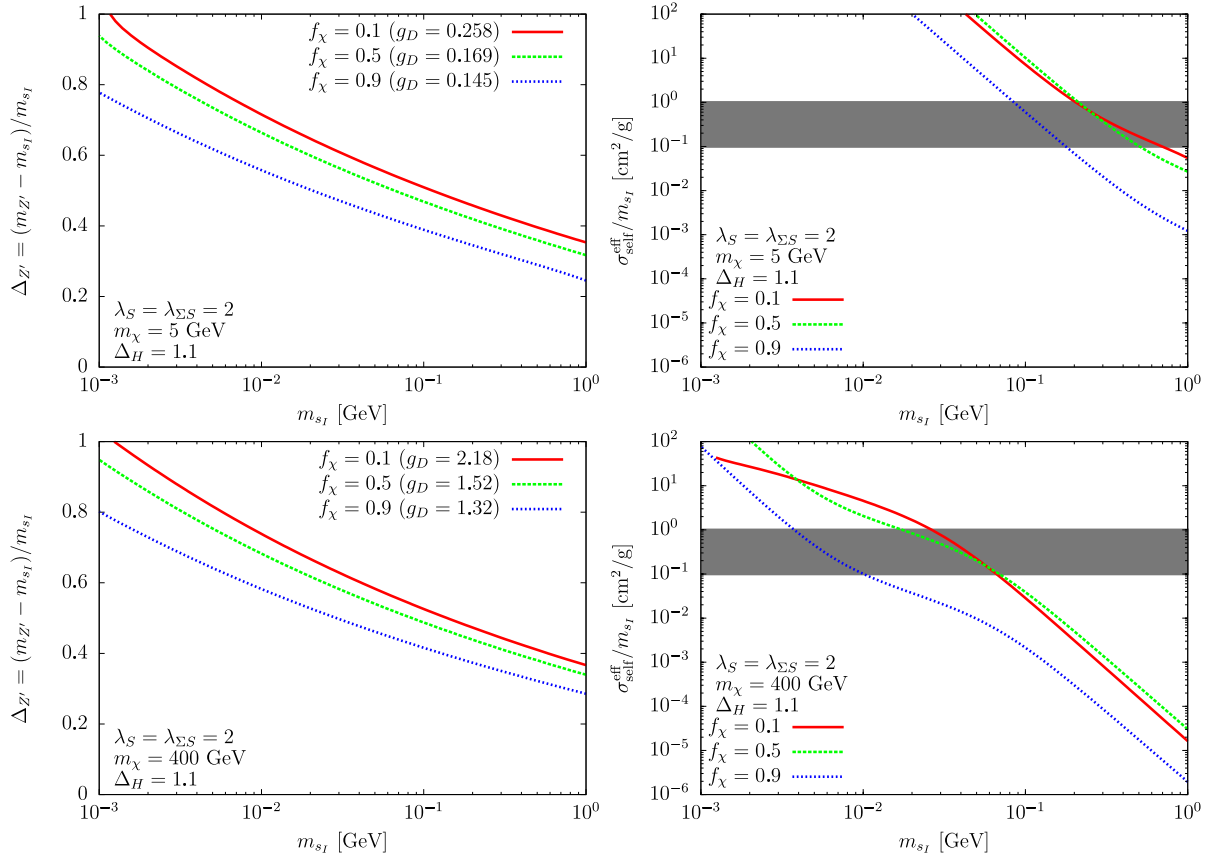


Figure 5: (left panels): Contours of the parameters satisfying the dark matter relic density in the $(m_{s_I}, \Delta_{Z'})$ plane. For each colored line, the fraction of two dark matter components are fixed as shown in the plots. The relevant parameters are fixed to be $\lambda_{\Sigma S} = \lambda_S = 2$, $\Delta_H = 1.1$ and $m_\chi = 5$ GeV (upper plots) or 400 GeV (lower plots). (right panels): The effective self-interacting cross section as a function of m_{s_I} where the colored lines correspond to the same colored lines in the left plots.

enough ($m_{Z'} \ll m_\chi$), the relic density of the heavier dark matter component χ is almost determined by two parameters, g_D and m_χ . Thus the hidden gauge coupling g_D is also fixed for each colored line to get the fixed fraction f_χ .

From the plots, one can see that the Z' mass should be $m_{Z'} \lesssim 2m_{s_I}$ ($\Delta_{Z'} \lesssim 1$). In this parameter set, the forbidden channel $SS^\dagger \rightarrow Z'Z'$ is dominant in most of the parameter region since the dark Higgs mass is fixed to be $m_H = 2.1m_S$ ($\Delta_H = 1.1$) which is too heavy to induce the forbidden channel $SS^\dagger \rightarrow HH$. In addition, one can see that the required value of $\Delta_{Z'}$ becomes smaller for heavier m_S . This is because the thermally averaged cross section $\langle\sigma v\rangle_{SS^\dagger \rightarrow Z'Z'}$ given by Eq. (24) is roughly scaled as $\langle\sigma v\rangle_{SS^\dagger \rightarrow Z'Z'} \sim e^{-2\Delta_{Z'}zs}/m_S^2$, which should be almost constant to explain the observed relic density. Therefore the decrease in the cross section due to heavier m_S must be compensated by the reduction of $\Delta_{Z'}$.

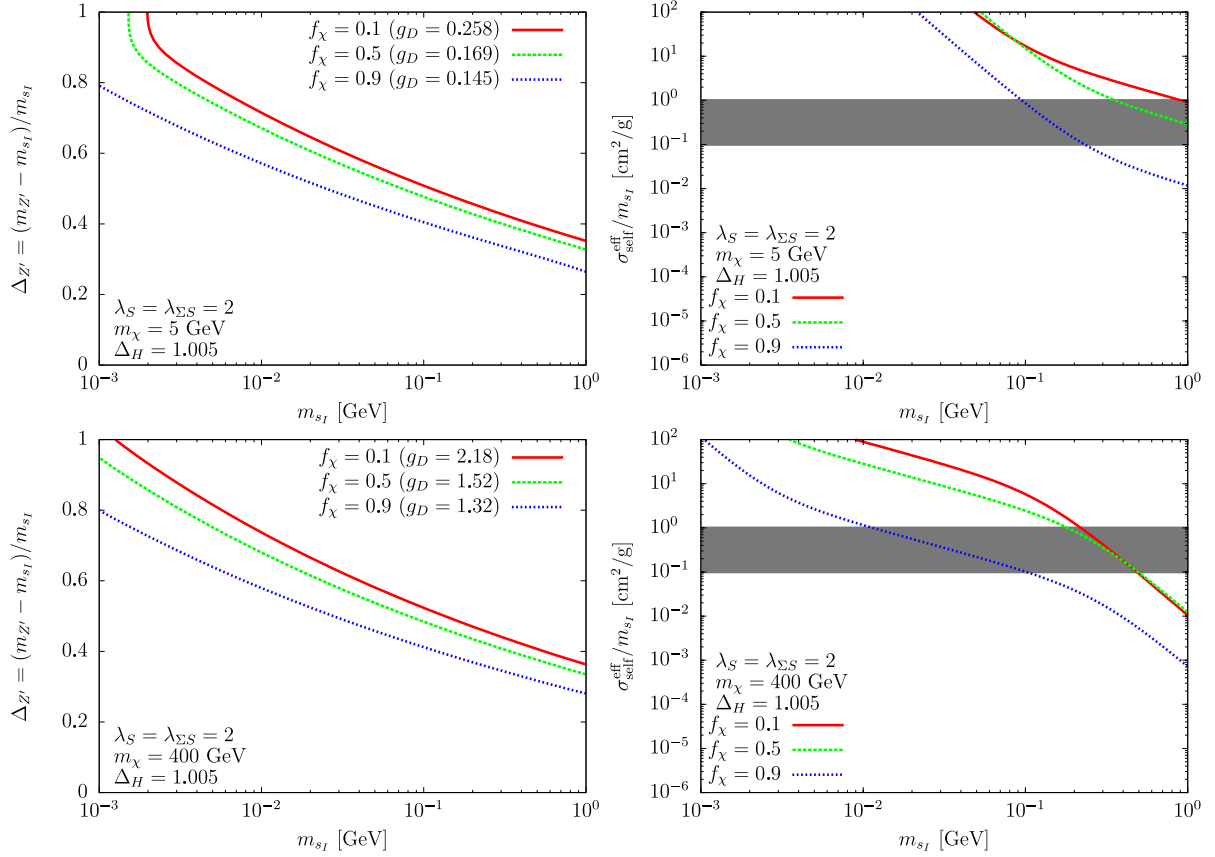


Figure 6: Same plots as Fig. 5 but for $\Delta_H = 1.005$.

In the right plots in Fig. 5, the effective self-interacting cross section $\sigma_{\text{self}}^{\text{eff}}/m_{s_I}$ is shown as a function of m_{s_I} for $f_\chi = 0.1, 0.5$ and 0.9 . The relevant parameter set is the same with the left plots. The self-interacting cross section as large as $0.1 \text{ cm}^2/\text{g} \leq \sigma_{\text{self}}^{\text{eff}}/m_{s_I} \leq 1 \text{ cm}^2/\text{g}$ can be obtained around $m_{s_I} \sim \mathcal{O}(100)$ MeV for $m_\chi = 5$ GeV and $m_{s_I} \sim 3 - 80$ MeV for $m_\chi = 400$ GeV. As can be seen in the left plots in Fig. 5, the Z' mass can be $\mathcal{O}(1 - 100)$ MeV to obtain the relic density consistent with the observed value.

The numerical results with $\Delta_H = 1.005$ are shown in Fig. 6. Taking $\Delta_H = 1.005$ means that the mass of the dark Higgs boson is close to the resonance $2m_{s_I} \approx m_H$. Thus the self-interacting cross section given by Eq. (40) can be enhanced as one can see from Fig. 5 and Fig. 6. We stress that the parameter region which can reproduce the appropriate value of the effective self-interacting cross section is shifted to heavier m_{s_I} . As a result, it is possible to take $m_{s_I}, m_{Z'}, m_H = \mathcal{O}(100)$ MeV even for $m_\chi = 400$ GeV.

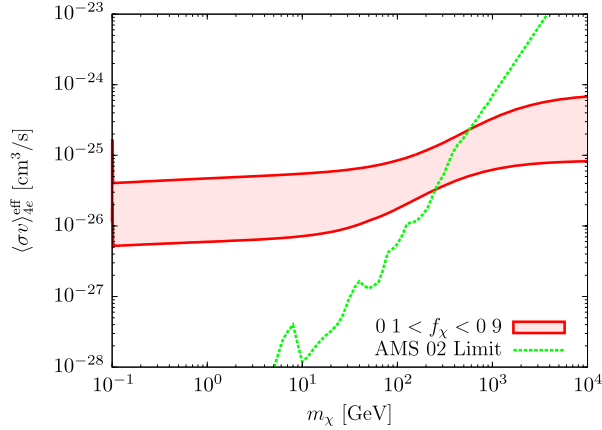


Figure 7: AMS-02 constraint where the upper region of the green line is excluded.

4 Detection Properties

4.1 Indirect Detection

In this model, the energetic e^\pm are produced through the annihilation of the heavier dark matter particle $\chi\chi^\dagger \rightarrow Z'Z' \rightarrow e^+e^-e^+e^-$ because the main decay mode of the Z' gauge boson is $Z' \rightarrow e^+e^-$.⁷ Furthermore, the annihilation cross section for this channel is enhanced by the Sommerfeld effect of the light mediator Z' . Thus, as can be seen in Eq. (35), the parameters m_χ and g_D relevant to the annihilation cross section of χ are strongly constrained by the AMS-02 positron observation [57]. The constraints on the annihilation cross sections for the specific channels such as e^+e^- , $\mu^+\mu^-$, $\tau^+\tau^-$, $b\bar{b}$, W^+W^- are given in Ref. [58], and the constraint for the final state e^+e^- is especially strong. In order to apply this bound for our case conservatively, we define the effective cross section into $e^+e^-e^+e^-$ by

$$\langle\sigma v\rangle_{4e}^{\text{eff}} \equiv 2 \left(\frac{\Omega_\chi}{\Omega_{\text{exp}}} \right)^2 \langle\sigma v\rangle_{\chi\chi^\dagger \rightarrow Z'Z'}, \quad (42)$$

where the factor 2 comes from two pairs of e^+e^- generated for each annihilation.⁸ We impose the constraint that this effective cross section should be smaller than the AMS-02 bound for the channel e^+e^- [58].

The bound for e^+e^- obtained by assuming the Einasto profile and the MED propagation model in Ref. [58] is translated into $e^+e^-e^+e^-$ as shown in Fig. 7. One should note that the upper bounds include some uncertainties such as the dark matter density profiles and the diffusion models. From Fig. 7, one can see that $m_\chi \gtrsim 800$ GeV is required to evade the AMS-02 constraint for $f_\chi = 0.9$, and $m_\chi \gtrsim 300$ GeV for $f_\chi = 0.1$. Thus the

⁷Depending on the Z' mass, the other decay channels are also possible such as $\mu^+\mu^-$ and $\pi^+\pi^-$.

⁸Precisely, since the energy of the produced positrons and electrons is different for e^+e^- and $e^+e^-e^+e^-$ final states, the translation of the bound for e^+e^- into $e^+e^-e^+e^-$ discussed here is not exactly true. Thus the obtained bound for $e^+e^-e^+e^-$ should be regarded as a conservative bound.

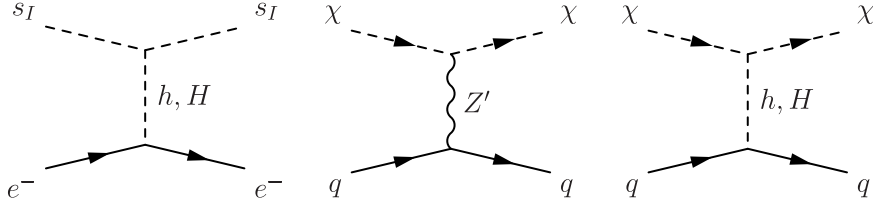


Figure 8: Diagrams for direct detection of dark matter s_I (left) and χ (centre and right).

mass of the dark matter component χ should be typically larger than the electroweak scale in order to satisfy $0.1 < f_\chi < 0.9$.

Due to this constraint, the numerical computations for $m_\chi = 5$ GeV in Fig. 5 and 6 are already excluded. For $m_\chi = 400$ GeV, only the blue line for $f_\chi = 0.9$ would be excluded. If a heavier m_χ is taken, f_χ can be larger, however a larger gauge coupling g_D is required to reproduce the correct relic density, which should be perturbative.

4.2 Direct Detection

Since the mass scale of the lighter dark matter particle s_I in this model is a few MeV to several hundred MeV, it would be difficult to detect it via direct detection with nuclei. However there is a chance to explore via direct detection with electron as shown in the left diagram in Fig. 8 where the elastic scattering of the lighter dark matter particle s_I with electron occurs via the Higgs couplings. The spin independent cross section is computed as

$$\sigma_{\text{DD}}^S = \frac{m_e^4}{4\pi(m_e + m_{s_I})^2} \left(\frac{\mu_{Hs_I s_I} \sin \alpha}{m_H^2 \langle \Phi \rangle} - \frac{\mu_{hs_I s_I} \cos \alpha}{m_h^2 \langle \Phi \rangle} \right)^2, \quad (43)$$

where $\mu_{hs_I s_I}$ ($= \mu_{hSS^\dagger}$) and $\mu_{Hs_I s_I}$ ($= \mu_{HSS^\dagger}$) are given by Eq. (19) and (30), respectively. The cross section is very suppressed by the electron Yukawa coupling (the electron mass). The scattering event with electron can be searched by direct detection experiments with current technology [59, 60]. The current strongest upper bound for the elastic cross section is given by XENON10 as $\sigma_{\text{DD}} \lesssim 10^{-38} \text{ cm}^2$ [61] at the dark matter mass of around 100 MeV. On the other hand, the typical order of the cross section given by Eq. (43) is $\sigma_{\text{DD}}^S \sim 10^{-45} \text{ cm}^2$ for $m_{s_I} \sim m_H \sim 100$ MeV and $\mu_{hs_I s_I} \sim \mu_{Hs_I s_I} \sim 1$ GeV, thus this constraint is easily satisfied. The experimental sensitivity can reach to the order of $\sigma_{\text{DD}} \sim 10^{-43} \text{ cm}^2$ with future experiments [59]. In particular, high sensitivity is achieved for the experiments using Germanium since the ionization threshold of Germanium is lower than the other elements such as Xenon and Argon.

For the heavier dark matter particle χ , since the mass should be above the electroweak scale as derived from the indirect detection constraint, the most stringent bound on the relevant parameters is given by the elastic scattering with a proton as shown in the centre and right diagrams in Fig. 8. The elastic scattering cross section for χ with a proton is

computed as

$$\sigma_{\text{DD}}^\chi = \frac{m_p^2}{16\pi (m_p + m_\chi)^2} \left[\frac{g_D e \epsilon_\gamma m_\chi}{m_{Z'}^2} + \left(\sum_q f_q^p \right) \left(\frac{\mu_{H\chi\chi^\dagger} \sin \alpha}{m_H^2} - \frac{\mu_{h\chi\chi^\dagger} \cos \alpha}{m_h^2} \right) \frac{2m_p}{\langle \Phi \rangle} \right]^2, \quad (44)$$

where m_p is the proton mass $m_p = 938$ MeV, the coefficient f_q^p is given in Ref. [62] and

$$\mu_{H\chi\chi^\dagger} = \sqrt{2} (-\lambda_{\Phi\chi} \langle \Phi \rangle \sin \alpha + \lambda_{\Sigma\chi} \langle \Sigma \rangle \cos \alpha). \quad (45)$$

The first and second terms in Eq. (44) correspond to the centre and right diagrams in Fig. 8, respectively. This spin independent cross section for χ is strongly constrained because the mediators Z' and H are much lighter than the dark matter mass m_χ . The effective spin-independent cross section defined by $\sigma_{\text{DD}}^\chi (\Omega_\chi / \Omega_{\text{exp}})$ should be compared with the experimental limits since the limits are derived for one-component dark matter. Under our assumptions $\lambda_{\Phi\chi}, \lambda_{\Sigma\chi} \ll 1$, we focus on the case that the Z' gauge boson contribution is dominant (the first term in Eq. (44)). In this case, the upper bound on the kinetic mixing ϵ_γ is obtained depending on the fraction f_χ of the total relic density as shown by the black lines in Fig. 9. The upper region of the black lines are excluded by the direct detection experiments. The colored regions, except for the green region, have already been excluded by the experiments (beam dump experiments [63], HPS [63], SN1987A [64], NA48/2 [65], Babar [66], MESA [67], SHiP [68]). The kinetic mixing gives a new contribution to anomalous magnetic moment of a charged lepton and the green region in Fig. 9 can account for the deviation between the experiment and the SM prediction for muon anomalous magnetic moment [69]. The required order of the kinetic mixing is roughly $\epsilon_\gamma \sim 10^{-3}$, while $\epsilon_\gamma \lesssim 10^{-7}$ or 10^{-8} is needed in our scenario of multi-component dark matter because of the strong direct detection bound for the heavier dark matter particle χ . In addition, the region of $\epsilon_\gamma \sim 10^{-3}$ has already been excluded by the other experiments.

In order to be consistent with getting the large self-interacting cross section for solving the small scale problems, $0.1 \text{ cm}^2/\text{g} \leq \sigma_{\text{self}}^{\text{eff}}/m_{s_I} \leq 1 \text{ cm}^2/\text{g}$, we found in Section 3 that the mass of Z' gauge boson is $m_{Z'} \lesssim 1$ GeV. Fig. 9 shows that the kinetic mixing ϵ_γ should be $\epsilon_\gamma \sim 10^{-10} - 10^{-9}$ for $m_{Z'} \sim \mathcal{O}(100)$ MeV and $\epsilon_\gamma \sim 10^{-9} - 10^{-8}$ for $m_{Z'} \gtrsim \mathcal{O}(100)$ MeV with $0.1 < f_\chi < 0.9$. The region of $m_{Z'} \lesssim 50$ MeV is excluded by the constraint of SN1987A [64]. Even for such a small kinetic mixing, some parameter space with $m_{Z'}$ of several hundred MeV can be tested by the SHiP (Search for Hidden Particles) experiment which is a newly proposed proton beam on target (tungsten) experiment [68, 70]. One more point is that a cancellation between the two different contributions mediated by the Z' gauge boson and the Higgs bosons may be possible (see Eq. (44)). In this case, the strong upper bound for the kinetic mixing would partially be relaxed. Since the magnitude of the kinetic mixing ϵ_γ is very small, the dark matter particles cannot be in kinetic equilibrium with the SM particles via the kinetic mixing. Instead of that the thermalization with the SM particles is realized by the couplings in the scalar potential.

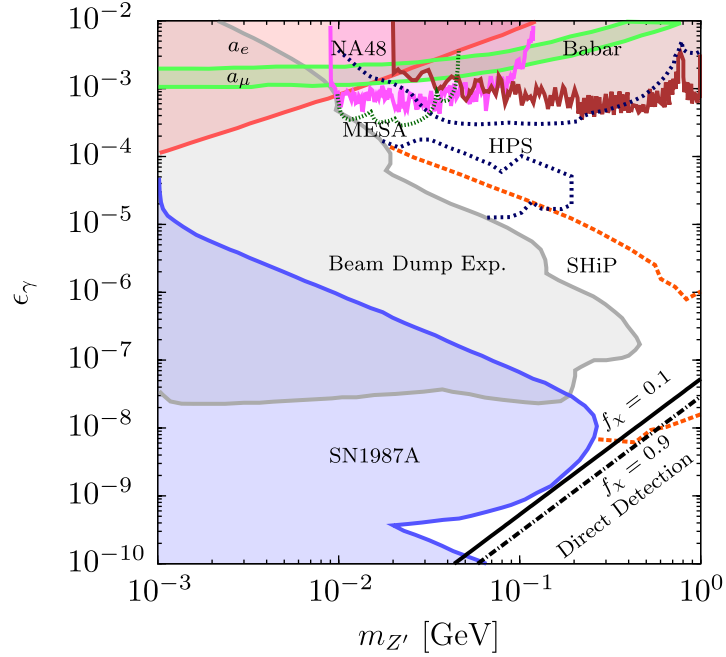


Figure 9: Current constraint on the kinetic mixing ϵ_γ and future sensitivities including beam dump experiments [63], HPS [63], SN1987A [64], NA48/2 [65], Babar [66], MESA [67], SHiP [68]. The black lines correspond to the upper bounds obtained by direct detection of the heavier dark matter particle χ when the Z' mediated contribution is dominant in Eq. (44).

5 Summary and Conclusions

We have considered the model extended with the hidden $U(1)_D$ gauge symmetry. Due to the remnant \mathbb{Z}_4 symmetry, the hidden scalar χ can be a dark matter candidate. In addition, since the decay of the light scalar s_I is kinematically forbidden, s_I can be a second dark matter component. We have discussed the phenomenology of the two dark matter components. The relic density of the lighter dark matter s_I can be determined by the forbidden channels into the Z' gauge boson and the extra dark Higgs boson H while that of the heavier state χ is dictated by the normal annihilation channel into the Z' gauge boson. In this framework, the mass scale of the lighter dark matter particle s_I is typically $1 \text{ MeV} \lesssim m_{s_I} \lesssim \mathcal{O}(100) \text{ MeV}$ and the couplings can be larger than the typical WIMP or WIMPless dark matter because the relic density of s_I is produced by forbidden channels, thus the lighter dark matter particle s_I can generate a large self-interacting cross section to solve the small scale problems of Λ CDM model.

We have also taken into account the constraints of indirect detection and direct detection of dark matter. From the constraint of indirect detection, the mass of the heavier dark matter state χ should be larger than electroweak scale. The constraint of direct detection for the heavier dark matter χ is very strong since the elastic scattering with a

nucleon can be induced by the light Z' gauge boson. To avoid this constraint, the kinetic mixing ϵ_γ and the scalar couplings between the heavier dark matter particle χ and the Higgs bosons should be very small. Nevertheless, if the Z' gauge boson is $m_{Z'} \gtrsim 200$ MeV and $\epsilon_\gamma \gtrsim 10^{-8}$, the model can be tested by the SHiP future experiment.

Acknowledgments

The work of M. A. is supported in part by the Japan Society for the Promotion of Sciences (JSPS) Grant-in-Aid for Scientific Research (Grant No. 25400250 and No. 16H00864). T. T. acknowledges support from P2IO Excellence Laboratory (LABEX) and JSPS Fellowships for Research Abroad. T. T. would like to thank Yann Mambrini for fruitful discussion.

References

- [1] O. D. Elbert, J. S. Bullock, S. Garrison-Kimmel, M. Rocha, J. Oñorbe and A. H. G. Peter, Mon. Not. Roy. Astron. Soc. **453**, no. 1, 29 (2015) [[arXiv:1412.1477](#) [astro-ph.GA]].
- [2] S. W. Randall, M. Markevitch, D. Clowe, A. H. Gonzalez and M. Bradac, Astrophys. J. **679**, 1173 (2008) [[arXiv:0704.0261](#) [astro-ph]].
- [3] R. Massey *et al.*, Mon. Not. Roy. Astron. Soc. **449**, no. 4, 3393 (2015) [[arXiv:1504.03388](#) [astro-ph.CO]].
- [4] F. Kahlhoefer, K. Schmidt-Hoberg, J. Kummer and S. Sarkar, Mon. Not. Roy. Astron. Soc. **452**, no. 1, L54 (2015) [[arXiv:1504.06576](#) [astro-ph.CO]].
- [5] Y. Hochberg, E. Kuflik, T. Volansky and J. G. Wacker, Phys. Rev. Lett. **113**, 171301 (2014) [[arXiv:1402.5143](#) [hep-ph]].
- [6] Y. Hochberg, E. Kuflik, H. Murayama, T. Volansky and J. G. Wacker, Phys. Rev. Lett. **115**, no. 2, 021301 (2015) [[arXiv:1411.3727](#) [hep-ph]].
- [7] N. Bernal, C. Garcia-Cely and R. Rosenfeld, JCAP **1504**, no. 04, 012 (2015) [[arXiv:1501.01973](#) [hep-ph]].
- [8] S. M. Choi and H. M. Lee, JHEP **1509**, 063 (2015) [[arXiv:1505.00960](#) [hep-ph]].
- [9] N. Bernal, X. Chu, C. Garcia-Cely, T. Hambye and B. Zaldivar, JCAP **1603**, no. 03, 018 (2016) [[arXiv:1510.08063](#) [hep-ph]].
- [10] N. Bernal and X. Chu, JCAP **1601**, 006 (2016) [[arXiv:1510.08527](#) [hep-ph]].
- [11] Y. Hochberg, E. Kuflik and H. Murayama, JHEP **1605**, 090 (2016) [[arXiv:1512.07917](#) [hep-ph]].
- [12] S. M. Choi and H. M. Lee, Phys. Lett. B **758**, 47 (2016) [[arXiv:1601.03566](#) [hep-ph]].

- [13] S. M. Choi, Y. J. Kang and H. M. Lee, JHEP **1612**, 099 (2016) [[arXiv:1610.04748](#) [hep-ph]].
- [14] J. L. Feng and J. Kumar, Phys. Rev. Lett. **101**, 231301 (2008) [[arXiv:0803.4196](#) [hep-ph]].
- [15] R. T. D’Agnolo and J. T. Ruderman, Phys. Rev. Lett. **115**, no. 6, 061301 (2015) [[arXiv:1505.07107](#) [hep-ph]].
- [16] A. Delgado, A. Martin and N. Raj, [arXiv:1608.05345](#) [hep-ph].
- [17] J. Fan, A. Katz, L. Randall and M. Reece, Phys. Dark Univ. **2**, 139 (2013) [[arXiv:1303.1521](#) [astro-ph.CO]].
- [18] J. Fan, A. Katz, L. Randall and M. Reece, Phys. Rev. Lett. **110**, no. 21, 211302 (2013) [[arXiv:1303.3271](#) [hep-ph]].
- [19] K. R. Dienes, J. Kumar, B. Thomas and D. Yaylali, Phys. Rev. Lett. **114**, no. 5, 051301 (2015) [[arXiv:1406.4868](#) [hep-ph]].
- [20] Y. Cai and A. P. Spray, JHEP **1601**, 087 (2016) [[arXiv:1509.08481](#) [hep-ph]].
- [21] M. Aoki, J. Kubo and H. Takano, Phys. Rev. D **87**, no. 11, 116001 (2013) [[arXiv:1302.3936](#) [hep-ph]].
- [22] Y. Kajiyama, H. Okada and T. Toma, Phys. Rev. D **88**, no. 1, 015029 (2013) [[arXiv:1303.7356](#) [hep-ph]].
- [23] M. Aoki, J. Kubo and H. Takano, Phys. Rev. D **90**, no. 7, 076011 (2014) [[arXiv:1408.1853](#) [hep-ph]].
- [24] W. Wang and Z. L. Han, Phys. Rev. D **92**, 095001 (2015) [[arXiv:1508.00706](#) [hep-ph]].
- [25] S. Y. Ho, T. Toma and K. Tsumura, Phys. Rev. D **94**, no. 3, 033007 (2016) [[arXiv:1604.07894](#) [hep-ph]].
- [26] R. Foot and S. Vagnozzi, Phys. Rev. D **91**, 023512 (2015) [[arXiv:1409.7174](#) [hep-ph]].
- [27] C. Gross, O. Lebedev and Y. Mambrini, JHEP **1508**, 158 (2015) [[arXiv:1505.07480](#) [hep-ph]].
- [28] G. Arcadi, C. Gross, O. Lebedev, Y. Mambrini, S. Pokorski and T. Toma, JHEP **1612**, 081 (2016) [[arXiv:1611.00365](#) [hep-ph]].
- [29] S. Bhattacharya, A. Drozd, B. Grzadkowski and J. Wudka, JHEP **1310**, 158 (2013) [[arXiv:1309.2986](#) [hep-ph]].
- [30] A. Alves, D. A. Camargo, A. G. Dias, R. Longas, C. C. Nishi and F. S. Queiroz, JHEP **1610**, 015 (2016) [[arXiv:1606.07086](#) [hep-ph]].
- [31] M. Klasen, F. Lyonnet and F. S. Queiroz, [arXiv:1607.06468](#) [hep-ph].
- [32] D. Chialva, P. S. B. Dev and A. Mazumdar, Phys. Rev. D **87**, no. 6, 063522 (2013) [[arXiv:1211.0250](#) [hep-ph]].

- [33] M. Kawasaki, K. Kohri and T. Moroi, Phys. Rev. D **71**, 083502 (2005) [[astro-ph/0408426](#)].
- [34] K. Jedamzik, Phys. Rev. D **74**, 103509 (2006) [[hep-ph/0604251](#)].
- [35] T. Robens and T. Stefaniak, Eur. Phys. J. C **75**, 104 (2015) [[arXiv:1501.02234](#) [hep-ph]].
- [36] A. Falkowski, C. Gross and O. Lebedev, JHEP **1505**, 057 (2015) [[arXiv:1502.01361](#) [hep-ph]].
- [37] J.-T. Wei *et al.* [Belle Collaboration], Phys. Rev. Lett. **103**, 171801 (2009) [[arXiv:0904.0770](#) [hep-ex]].
- [38] R. Aaij *et al.* [LHCb Collaboration], JHEP **1302**, 105 (2013) [[arXiv:1209.4284](#) [hep-ex]].
- [39] J. P. Lees *et al.* [BaBar Collaboration], Phys. Rev. D **87**, no. 3, 031102 (2013) Erratum: [Phys. Rev. D **87**, no. 5, 059903 (2013)] [[arXiv:1210.0287](#) [hep-ex]].
- [40] K. Schmidt-Hoberg, F. Staub and M. W. Winkler, Phys. Lett. B **727**, 506 (2013) [[arXiv:1310.6752](#) [hep-ph]].
- [41] G. Aad *et al.* [ATLAS Collaboration], JHEP **1601**, 172 (2016) [[arXiv:1508.07869](#) [hep-ex]].
- [42] V. Khachatryan *et al.* [CMS Collaboration], [arXiv:1610.09218](#) [hep-ex].
- [43] LHC Higgs Cross Section Working Group, <https://twiki.cern.ch/twiki/bin/view/LHCPhysics/CERNYellowReportPageBR>.
- [44] K. Griest and D. Seckel, Phys. Rev. D **43**, 3191 (1991).
- [45] J. Hisano, S. Matsumoto, M. Nagai, O. Saito and M. Senami, Phys. Lett. B **646**, 34 (2007) [[hep-ph/0610249](#)].
- [46] J. Hisano, S. Matsumoto and M. M. Nojiri, Phys. Rev. D **67**, 075014 (2003) [[hep-ph/0212022](#)].
- [47] J. Hisano, S. Matsumoto and M. M. Nojiri, Phys. Rev. Lett. **92**, 031303 (2004) [[hep-ph/0307216](#)].
- [48] J. Hisano, S. Matsumoto, M. M. Nojiri and O. Saito, Phys. Rev. D **71**, 063528 (2005) [[hep-ph/0412403](#)].
- [49] J. Hisano, S. Matsumoto, O. Saito and M. Senami, Phys. Rev. D **73**, 055004 (2006) [[hep-ph/0511118](#)].
- [50] J. L. Feng, M. Kaplinghat and H. B. Yu, Phys. Rev. D **82**, 083525 (2010) [[arXiv:1005.4678](#) [hep-ph]].
- [51] L. G. van den Aarssen, T. Bringmann and C. Pfrommer, Phys. Rev. Lett. **109**, 231301 (2012) [[arXiv:1205.5809](#) [astro-ph.CO]].

- [52] S. Tulin, H. B. Yu and K. M. Zurek, Phys. Rev. Lett. **110**, no. 11, 111301 (2013) [[arXiv:1210.0900](#) [hep-ph]].
- [53] T. R. Slatyer, N. Padmanabhan and D. P. Finkbeiner, Phys. Rev. D **80**, 043526 (2009) [[arXiv:0906.1197](#) [astro-ph.CO]].
- [54] J. Zavala, M. Vogelsberger and S. D. M. White, Phys. Rev. D **81**, 083502 (2010) [[arXiv:0910.5221](#) [astro-ph.CO]].
- [55] J. Hisano, M. Kawasaki, K. Kohri, T. Moroi, K. Nakayama and T. Sekiguchi, Phys. Rev. D **83**, 123511 (2011) [[arXiv:1102.4658](#) [hep-ph]].
- [56] M. Kawasaki, K. Kohri, T. Moroi and Y. Takaesu, Phys. Lett. B **751**, 246 (2015) [[arXiv:1509.03665](#) [hep-ph]].
- [57] M. Aguilar *et al.* [AMS Collaboration], Phys. Rev. Lett. **110**, 141102 (2013).
- [58] A. Ibarra, A. S. Lamperstorfer and J. Silk, Phys. Rev. D **89**, no. 6, 063539 (2014) [[arXiv:1309.2570](#) [hep-ph]].
- [59] R. Essig, J. Mardon and T. Volansky, Phys. Rev. D **85**, 076007 (2012) [[arXiv:1108.5383](#) [hep-ph]].
- [60] Y. Hochberg, Y. Zhao and K. M. Zurek, Phys. Rev. Lett. **116**, no. 1, 011301 (2016) [[arXiv:1504.07237](#) [hep-ph]].
- [61] R. Essig, A. Manalaysay, J. Mardon, P. Sorensen and T. Volansky, Phys. Rev. Lett. **109**, 021301 (2012) [[arXiv:1206.2644](#) [astro-ph.CO]].
- [62] J. M. Cline, K. Kainulainen, P. Scott and C. Weniger, Phys. Rev. D **88**, 055025 (2013) Erratum: [Phys. Rev. D **92**, no. 3, 039906 (2015)] [[arXiv:1306.4710](#) [hep-ph]].
- [63] R. Essig *et al.*, [arXiv:1311.0029](#) [hep-ph].
- [64] D. Kazanas, R. N. Mohapatra, S. Nussinov, V. L. Teplitz and Y. Zhang, Nucl. Phys. B **890**, 17 (2014) [[arXiv:1410.0221](#) [hep-ph]].
- [65] J. R. Batley *et al.* [NA48/2 Collaboration], Phys. Lett. B **746**, 178 (2015) [[arXiv:1504.00607](#) [hep-ex]].
- [66] J. P. Lees *et al.* [BaBar Collaboration], Phys. Rev. Lett. **113**, no. 20, 201801 (2014) [[arXiv:1406.2980](#) [hep-ex]].
- [67] T. Beranek, H. Merkel and M. Vanderhaeghen, Phys. Rev. D **88**, 015032 (2013) [[arXiv:1303.2540](#) [hep-ph]].
- [68] S. Alekhin *et al.*, Rept. Prog. Phys. **79**, no. 12, 124201 (2016) [[arXiv:1504.04855](#) [hep-ph]].
- [69] H. S. Lee, Phys. Rev. D **90**, no. 9, 091702 (2014) [[arXiv:1408.4256](#) [hep-ph]].
- [70] D. Gorbunov, A. Makarov and I. Timiryasov, Phys. Rev. D **91**, no. 3, 035027 (2015) [[arXiv:1411.4007](#) [hep-ph]].